Beam Physics Note 6

December 17, 1998
`kaltchev@cern.ch`

Present situation of the cleaning insertions IR3 and IR7

J.B. Jeanneret, D. Kaltchev, A. Verdier

Keywords: `collimation, lattices, linear optics`

The lattices described here are matched to LHC version V6.-2. The main quadrupole strengths used in the next two sections are:

```
Main quads:

KQF :=  .0087696
KQD := -.0085463
```

1 IR3

The preferred layout is:
- Q6 cold
- 2 polarities of warm quadrupoles MQW, i.e. addition of a symmetric element to the MQW's
- standard main quads in the DS

Reasons:

1) Q6 cold is the only solution which provides DXN= $D_x/\sqrt{\beta_x}$ above 0.2 $m^{1/2}$ (0.22 $m^{1/2}$ reached, Fig 1). Q6 is composed of a standard cold main quad and 2 trims of length 1.15 m.

2) The addition of a symmetric element to the MQW's is mandatory to maintain the strength of QT12.L3 below the limit and the strength of the MQW's below 0.0015 m^{-2}.

3) With an exact antisymmetry of the MQW's (without symmetric elements) the trim strengths can not be reduced to acceptable values even by introducing MQL in the IR3 DS.

Fig 1 shows an IR3 lattice with Q6 cold and with symmetric MQW's (quad strengths KQ6S.3, KQ5S.3, KQ4S.3). The corresponding table shows the K1 values of the Q6-trims, warm and DS-trim quads, in this order. There are 24 warm modules, of them 4 of the

F and D remind you the nearest main quad polarity. A higher DXN peak is impossible to get because KQT12.L3 exceeds 0.0047 m^{-2} (110 T/m).

Fig 2 shows IR3 lattice with Q6 warm and symmetric MQW's. The location of the DXN (=0.18) peak is tuned to be located between the dogleg magnets.

Fig 3 shows the same case of warm Q6, but without symmetric MQW's (set to zero). Here KQT8.L3, KQT10.L3 , KQT12.L3 (all "F") exceed twice the allowed limit (=0.0047). For the first two, increasing the corresponding main quad lengths from 3.1m to 3.45m will not help because this would contribute only $0.00877 * 0.35/1.15 = 0.0027$ to the K1 values. The length of the main quad Q12, cannot be increased.

2 IR7

The preferred layout is:

- Q6 cold

- 2 polarities of warm quadrupoles MQW, i.e. addition of a symmetric element to the MQW's

- standard main quads in the DS

Reasons:

1) Q6 cold is the only solution which provides a dispersion D<25 cm in the straight section. With Q6 warm, we get $D \sim -100$ cm at some location, while the maximum allowed is $\sim$ 40cm.

2) having Q6 cold and addition of a symmetric element to the MQW's provides a larger asymmetry near the middle of the insertion, which is an important ingredient for efficient collimation. Such an increased asymmetry is more important than a net increase of the total available phase advance interval (as in case of Q6 warm).

Simulations using the code DJ show that the collimation quality can be related to the shape of the tune-split function measured from the location of the primary collimators:
$\mu_y(\mu_x)$ $(\mu_y = \mu_x = 0$ at the primary),
or equally:
$(\mu_y - \mu_x)/2$ depending on $(\mu_y + \mu_x)/2$.
The four primary jaw-collimators are located within the drift of the left dogleg.
The value of the escaping amplitudes is related to the shape and the position of the curve $\mu_y(\mu_x)$ with respect to the optimum contours $A(\mu_x, \mu_y) = 1$ corresponding to a secondary amplitude normalized to a secondary collimator aperture. In case of Q6 cold and in presence of symmetric modules this shape can be made more irregular by increasing the symmetric parts: KQ4S and KQ5S. Having such an irregular shape and the ability to control it is the preferable option.
In the limiting case of exactly regular $(\mu_y - \mu_x)/2$, the phases above 0.5 $(\times 2\pi)$ are not used, because the conditions for collimation repeat itself with the periodicity of the contours

Fig 4 shows the case Q6 cold and symmetric modules. The tune interval available for secondary jaws is $0.002 < \mu_x < 0.587$. The results are:

16 jaws: $A_{max} = 8.9$, $A_{x,max} = 8$, $A_{y,max} = 7.7$

Fig 5 shows the case Q6 warm and symmetric modules. The tune interval available for secondary jaws is larger: $0.002 < \mu_x < 0.8$. The result is:

16 jaws: $A_{max} = 8.9$, $A_{x,max} = 8.8$, $A_{y,max} = 8.4$

Fig 6 shows the case Q6 warm and symmetric modules set to zero.

Fig 7 shows the case Q6 cold with symmetric modules set to zero. The result is:

16 jaws: $A_{max} = 9.2$ $A_{x,max} = 8.35$ $A_{y,max} = 7.87$

These survivng amplitudes are larger than in the case of Q6 cold and nonzero symmetric modules.

3 Lattices matched to arc with cell tunes $\mu_{x,cell} = 0.28 = \frac{7}{25}$, $\mu_{y,cell} = 0.24 = \frac{6}{25}$

The main quadrupole strengths are:

```
Main quads:

KQF :=  .0091824
KQD := -.0084275
```

Two cases were considered :

Fig 8 (/ir3/q6cold) and

Fig 9 (/ir7/q6cold).

DJ analizys is not yet done, but the optics in both cases looks adequate for colliation.

4 Conclusions

In both IR3 and IR7, the requested performance of the insertion to do good collimation implies

- The use of a cold Q6 made of a regular arc quadrupole (MQ,3.1m long)) and of two TRIM's 1.15m long.
- The use of an additional 'symmetric' MQW (same hardware, electric cabling modified), for a total number of 24 MQW modules in each insert ion.

With this option, regular MQ (3.1m long) and short trim's (1.15m long) can be used in the dispersion suppressors.

In IR3, the present limit towards better performance is the strength of MQ12.

In IR7, the present limit towards better performance is the strength of both MQ12 and MQ7, the latter one being easy to overcome (space fo r a second trim exists).

Would Q6 be warm, the number of MQW modules would be 38 in IR3 and 42 in IR7.

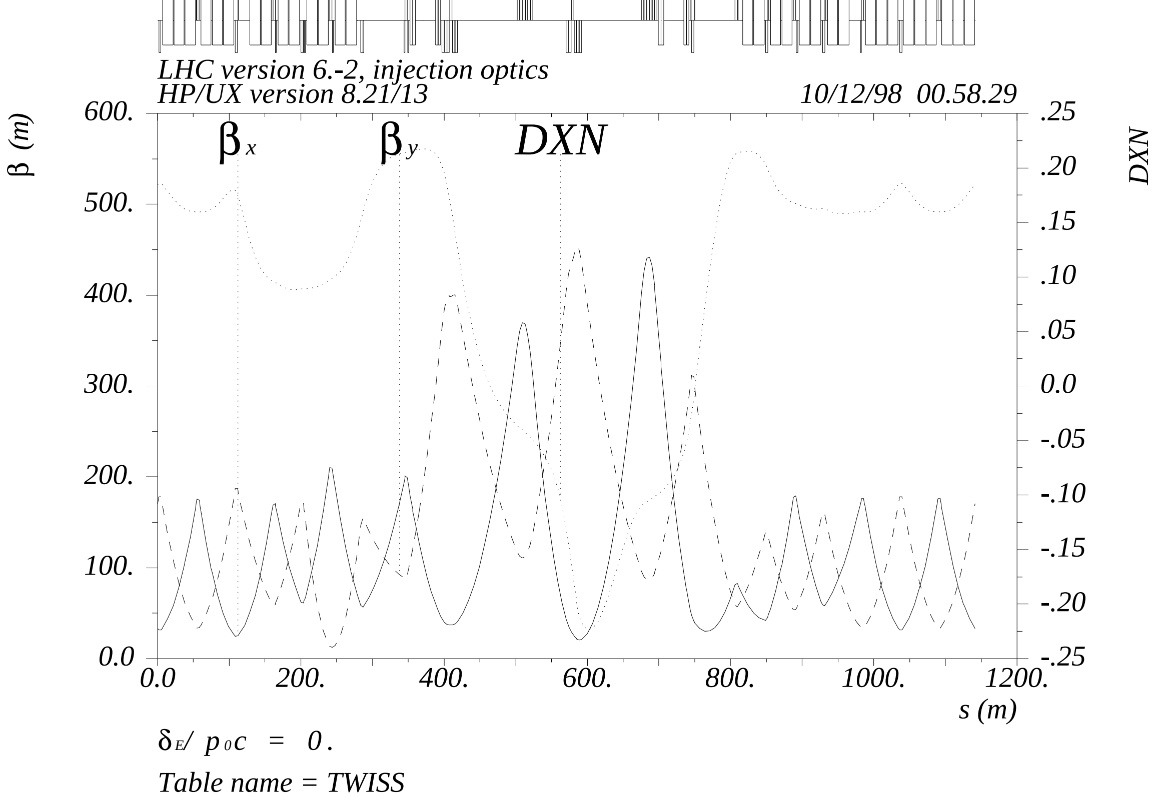

Fig 1: /ir3/q6cold

KQT6.R3	.0030790
KQT6.L3	-.0024657
KQ5A.3	-.0012874
KQ5S.3	.0011948
KQ4A.3	.0012231
KQ4S.3	.0010519
KQT12.L3	.0043824
KQT11.L3	.0027619
KQT10.L3	-.0000679
KQT9.L3	-.0036215
KQT8.L3	-.0011485
KQT7.L3	-.0012736
KQT11.R3	-.0033986
KQT10.R3	.0008716
KQT9.R3	-.0000325
KQT8.R3	.0033000
KQT7.R3	.0008228

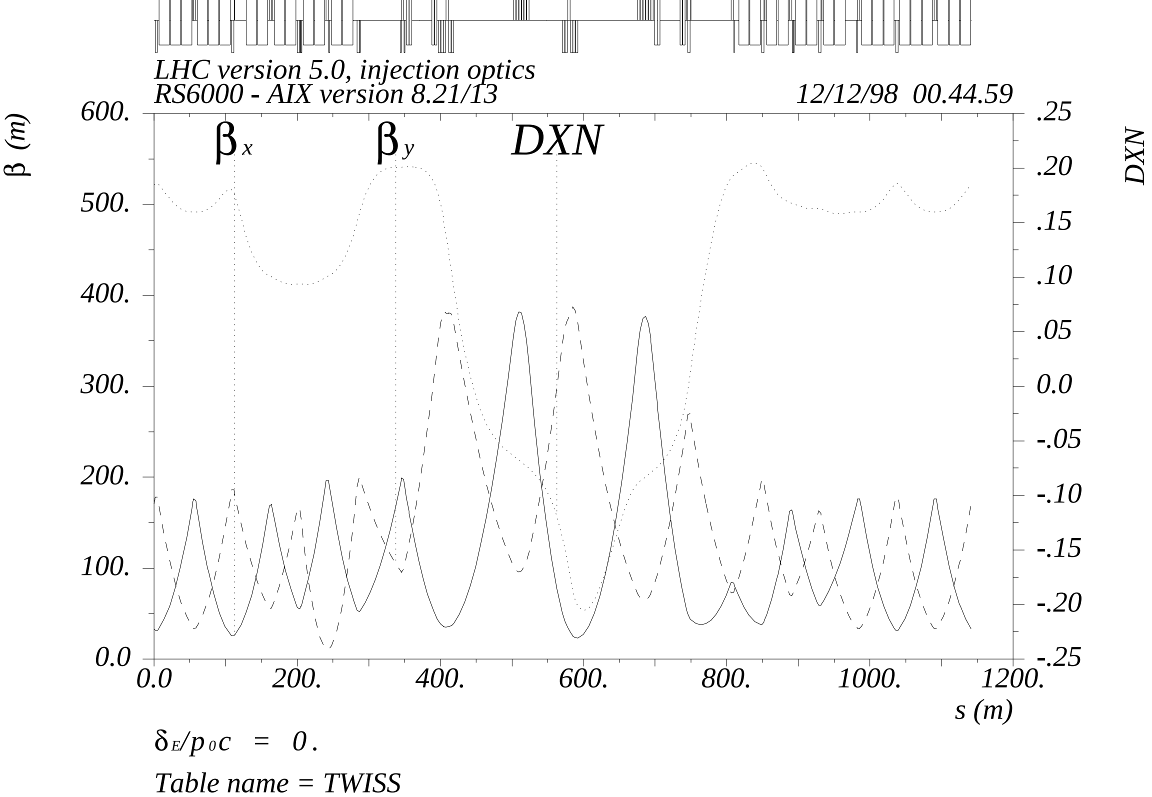


```
Fig 1a: /ir3/q6cold with aperture limitations:
betamax at Q5A.R3 reduced by 40m; DXN = 0.2

 KQT6.R3       0.0033112
 KQT6.L3        -0.0021544

 KQ5A.3         -0.0012681
 KQ5S.3        0.0011446
 KQ4A.3        0.0012360
 KQ4S.3        0.0008785

 KQT12.L3      0.0039481
 KQT11.L3      0.0024340
 KQT10.L3      0.0005570
 KQT9.L3        -0.0044559
 KQT8.L3        -0.0004571
 KQT7.L3        -0.0014935
 KQT11.R3       -0.0035092
 KQT10.R3      0.0028607
 KQT9.R3        -0.0000706
 KQT8.R3       0.0035988
 KQT7.R3        -0.0004883
```

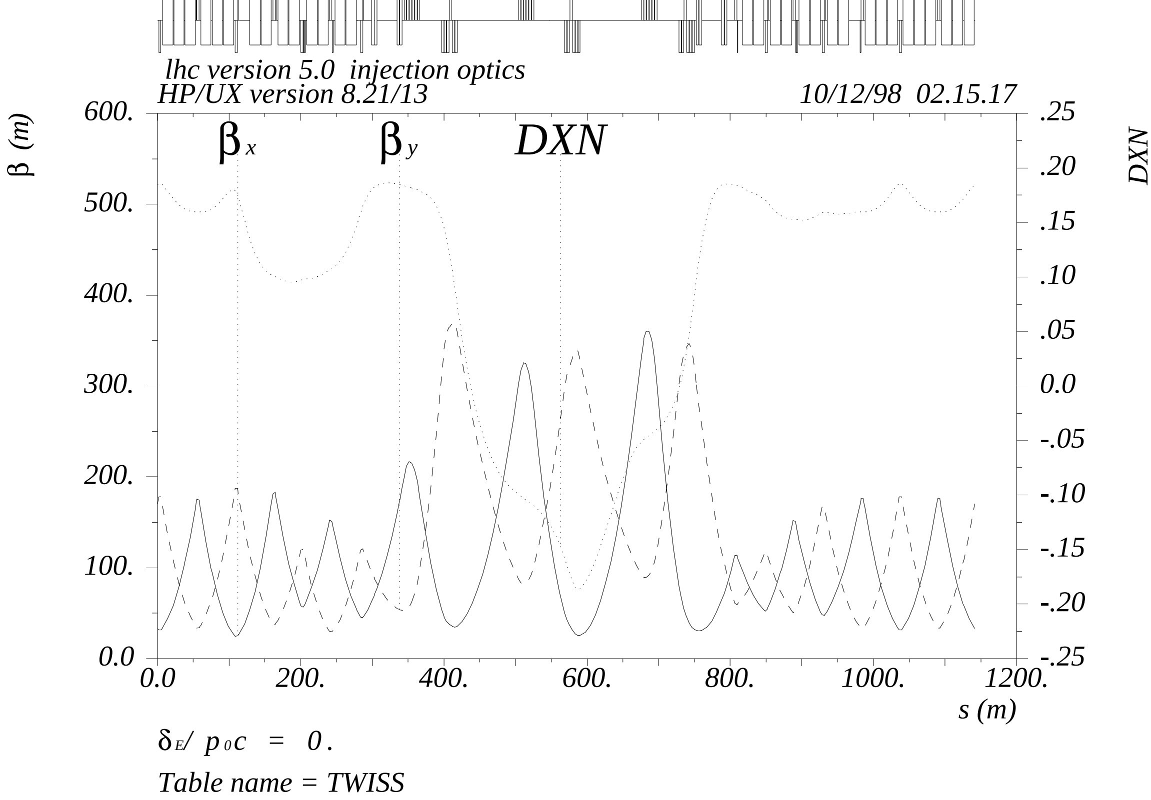

Fig 2: /ir3/q6warm

KQ6A.3	.0015480	> limit
KQ6S.3	.0005325	
KQ5A.3	-.0014881	near limit
KQ5S.3	.0007761	
KQ4A.3	.0012423	
KQ4S.3	.0010473	
KQT11.L3	.0004229	
KQT10.L3	.0008176	
KQT9.L3	-.0020552	
KQT8.L3	-.0020158	
KQT7.L3	.0011837	
KQT11.R3	-.0022599	
KQT10.R3	.0004091	
KQT9.R3	-.0007749	
KQT8.R3	.0048854	
KQT7.R3	-.0018727	

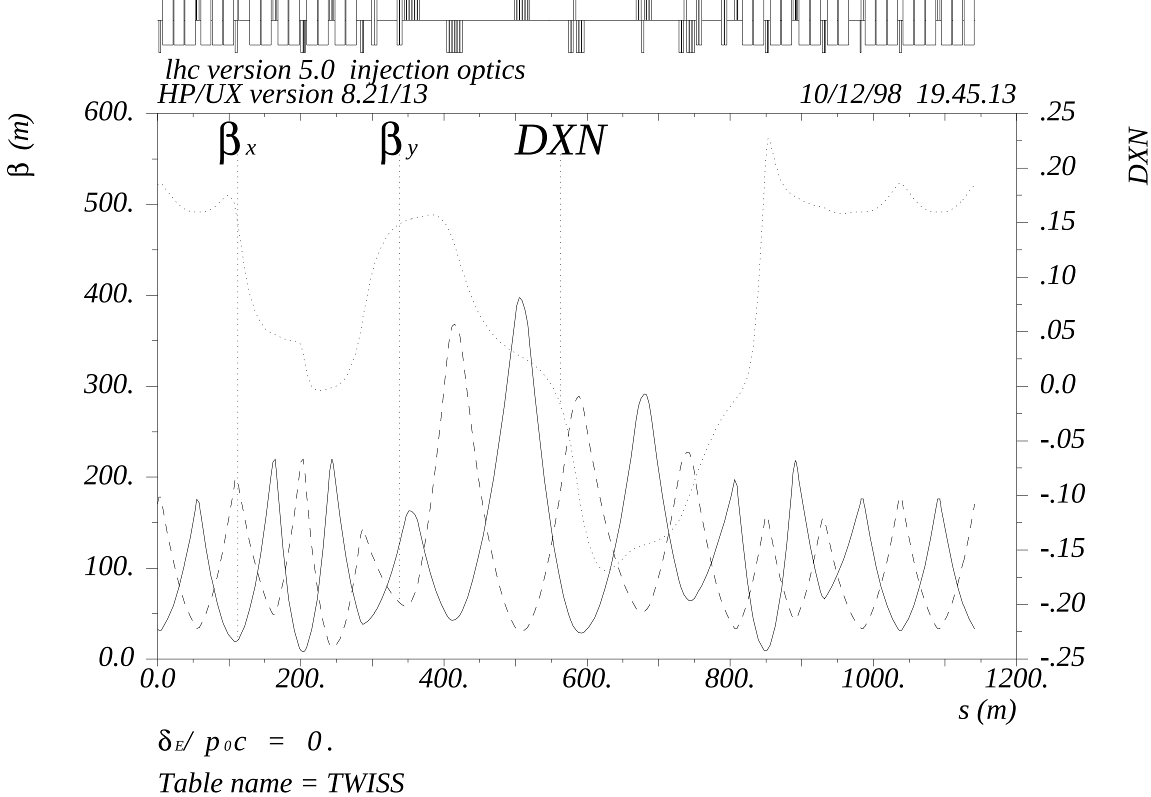

Fig 3: /ir3/q6warm with small or zero symmetric modules (KQ4S.3, KQ5S.3 and KQ6S.3)

KQ6A.3	.0015688	> limit
KQ6S.3	.0000357	
KQ5A.3	-.0014437	
KQ5S.3	-.0000051	
KQ4A.3	.0013369	
KQ4S.3	.0000443	

KQT12.L3	.0096773	> limit
KQT11.L3	.0016176	
KQT10.L3	.0118267	> limit
KQT9.L3	-.0046816	
KQT8.L3	.0111512	> limit
KQT7.L3	-.0043206	

KQT11.R3	-.0041398
KQT10.R3	-.0008230
KQT9.R3	.0040913
KQT8.R3	-.0030939
KQT7.R3	.0043593

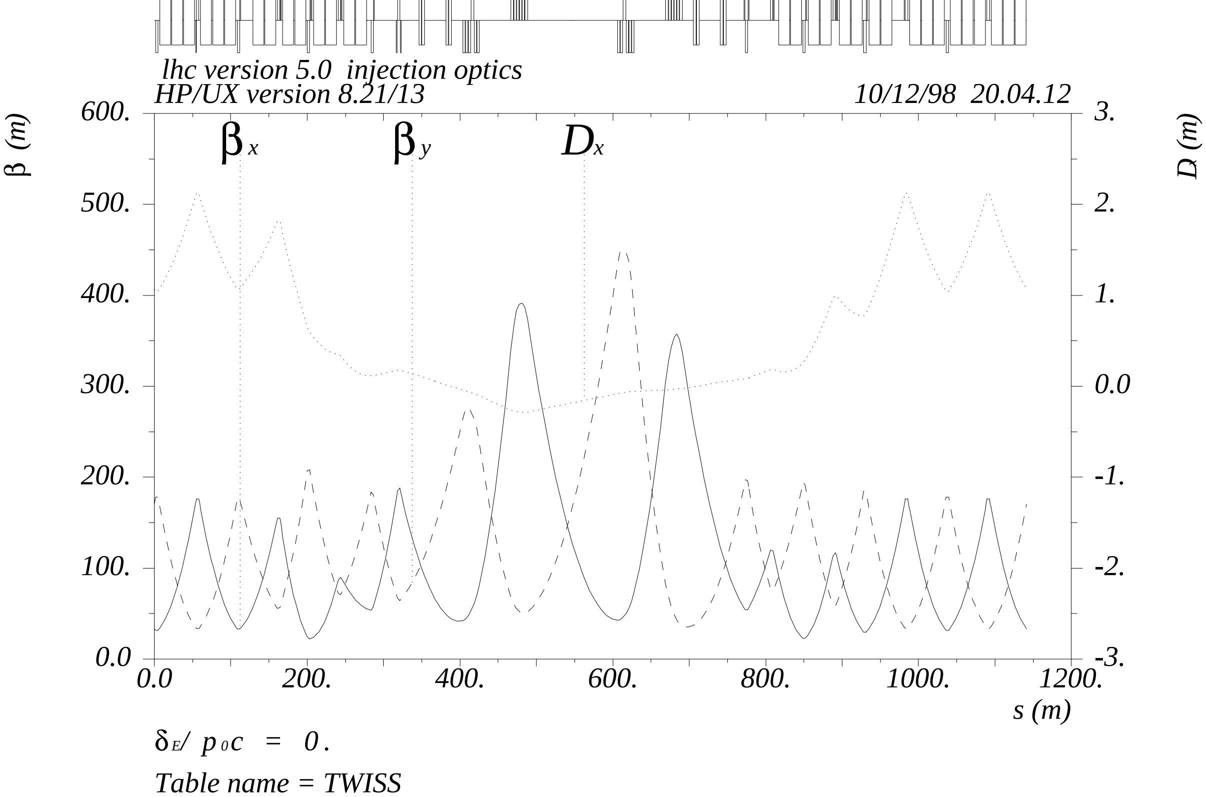

Fig 4: /ir7/q6cold

KQT6.R7	.0012646
KQT6.L7	-.0011484
KQ5A.7	-.0012706
KQ5S.7	.0002222
KQ4A.7	.0012553
KQ4S.7	.0000416

KQT12.L7	-.0007046
KQT11.L7	.0025927
KQT10.L7	.0045950
KQT9.L7	.0003270
KQT8.L7	.0014896
KQT7.L7	.0026132

KQT11.R7	.0002057
KQT10.R7	.0004712
KQT9.R7	.0036480
KQT8.R7	.0028023
KQT7.R7	.0031240

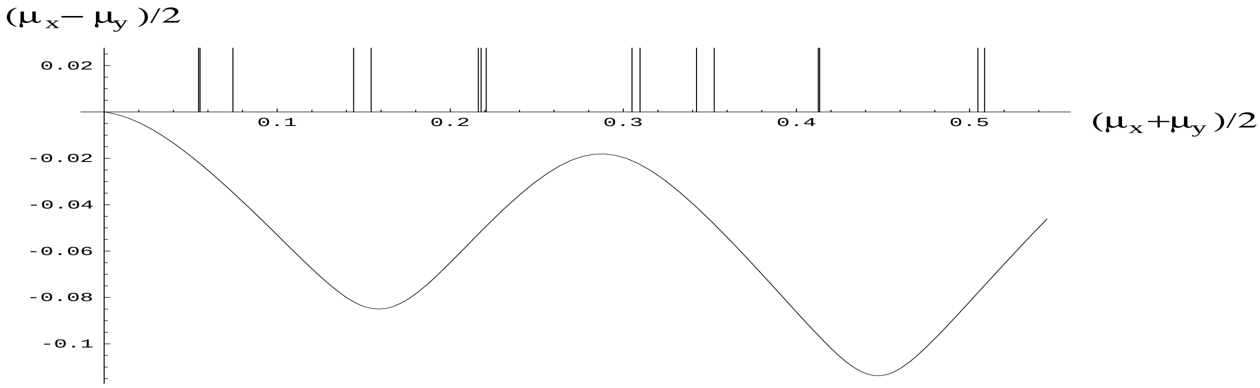

Figure 4 a) The split function $(\mu_y - \mu_x)/2$ vs $(\mu_y + \mu_x)/2$ for the lattice on Figure 4 (ir7/q6cold). At the primary collimator we choose to have $\mu_x = \mu_y$=0. The setup of 16 sec. jaws presented on the plot by vertical lines corepond to $A_{max} = 8.9$, $A_{x,max} = 7.95$, $A_{y,max} = 7.7$

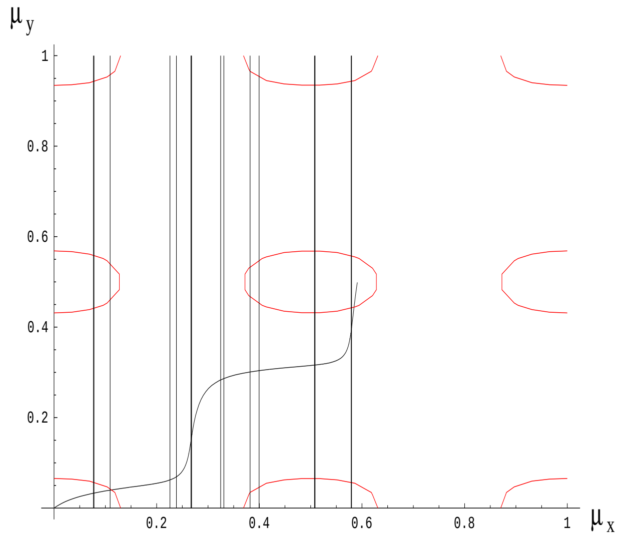

Figure 4 b) The split function, same as on the above plot, but on the plane μ_x,μ_y. At the primary collimator $\mu_x = \mu_y$=0. Collimation quality can be related to the position of the split curve with respect to the contours $A(\mu_x, \mu_y) = 1$, also shown.

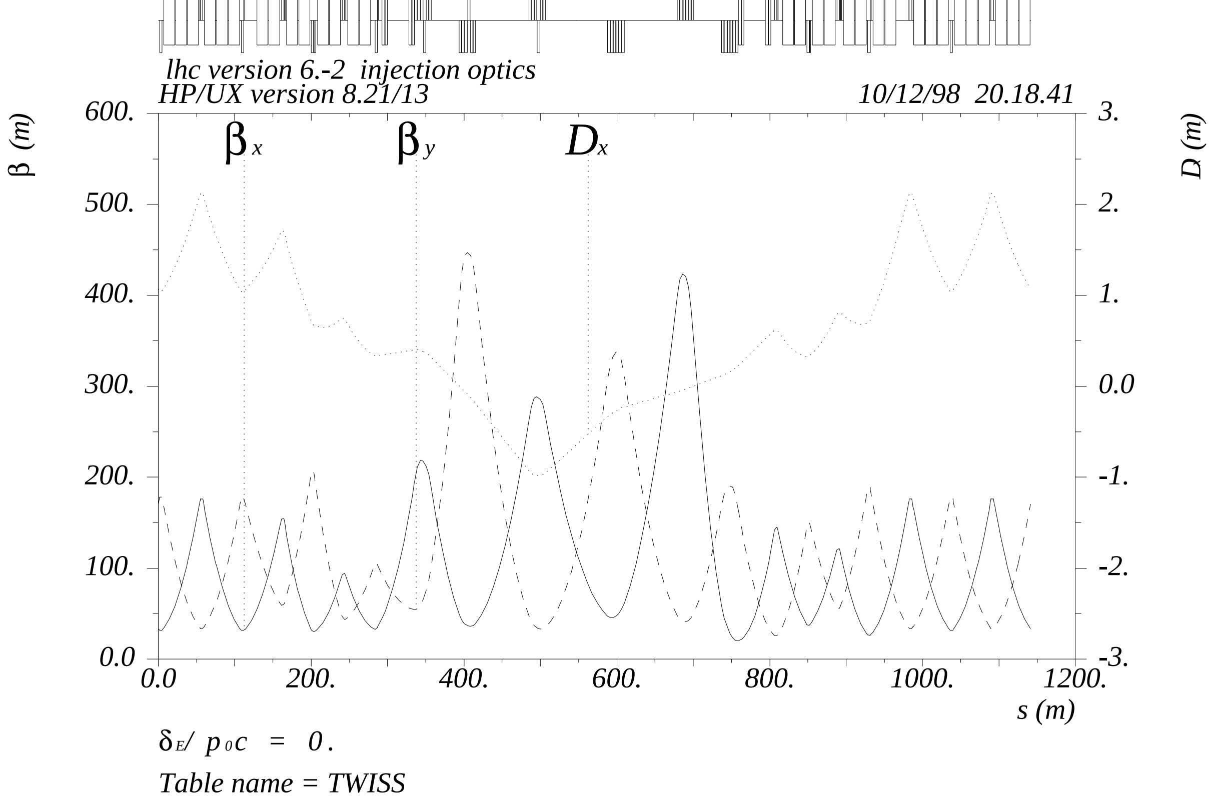

Fig 5: ir7/q6warm

KQ6A.7	.0017914	> limit
KQ6S.7	-.0001735	
KQ5A.7	-.0015492	> limit
KQ5S.7	.0002803	
KQ4A.7	.0012207	
KQ4S.7	-.0000509	
KQT12.L7	.0001529	
KQT11.L7	.0028953	
KQT10.L7	.0031035	
KQT9.L7	-.0009310	
KQT8.L7	.0034114	
KQT7.L7	.0044823	
KQT11.R7	.0007981	
KQT10.R7	.0000633	
KQT9.R7	.0023029	
KQT8.R7	-.0025714	
KQT7.R7	.0041087	

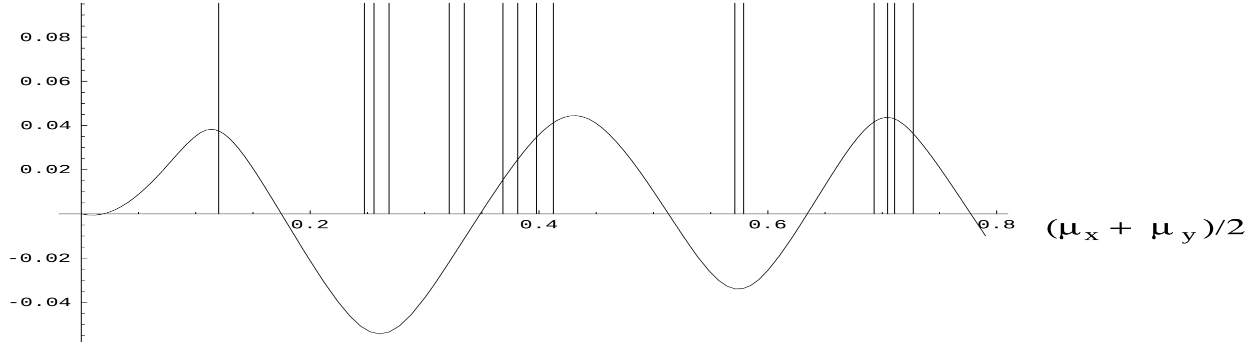

Figure 5 a) The split function $(\mu_y - \mu_x)/2$ vs $(\mu_y + \mu_x)/2$ for the lattice on Figure 5 (ir7/q6warm). At the primary collimator we choose to have $\mu_x = \mu_y$=0. The setup of 16 sec. jaws presented on the plot by vertical lines corespond to $A_{max} = 8.84$, $A_{x,max} = 8.8$, $A_{y,max} = 8.4$

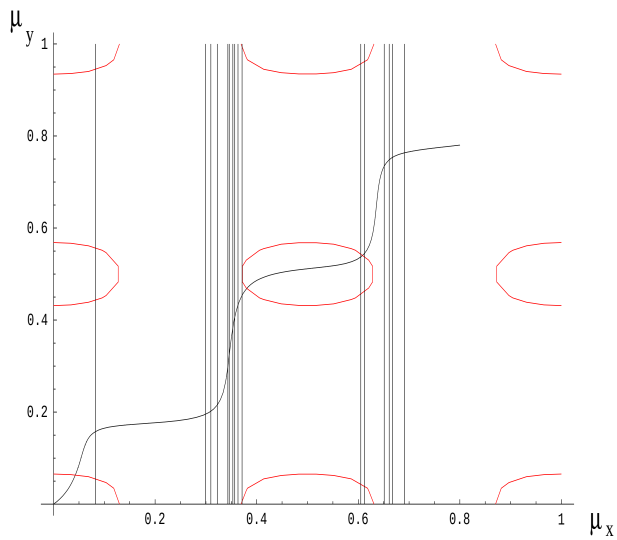

Figure 5 b) The split function, same as on the above plot, but on the plane μ_x,μ_y. At the primary collimator $\mu_x = \mu_y$=0. Collimation quality can be related to the position of the split curve with respect to the contours $A(\mu_x, \mu_y) = 1$, also shown.

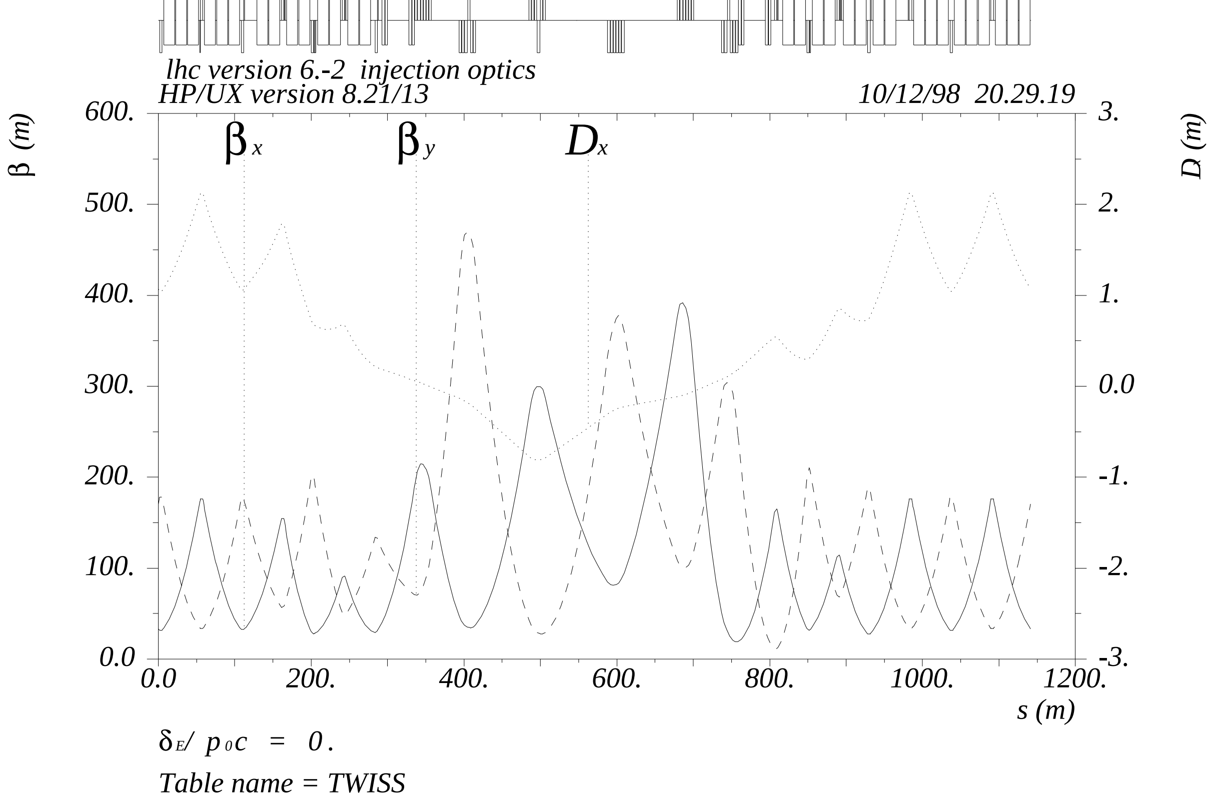

Fig 6: /ir7/q6warm with small or zero symmetric modules (KQ4S.7, KQ5S.7 and KQ6S.7)

```
KQ6A.7      .0018006      > limit
KQ6S.7      .0000088
KQ5A.7       -.0014955      near limit
KQ5S.7      .0001063
KQ4A.7      .0010854
KQ4S.7      .0000000

KQT12.L7     -.0004300
KQT11.L7    .0026983
KQT10.L7    .0033843
KQT9.L7      -.0006624
KQT8.L7     .0053666
KQT7.L7     .0060610       > limit

KQT11.R7    .0005081
KQT10.R7    .0015058
KQT9.R7     .0027048
KQT8.R7      -.0067280       > limit
KQT7.R7     .0050084        near limit
```

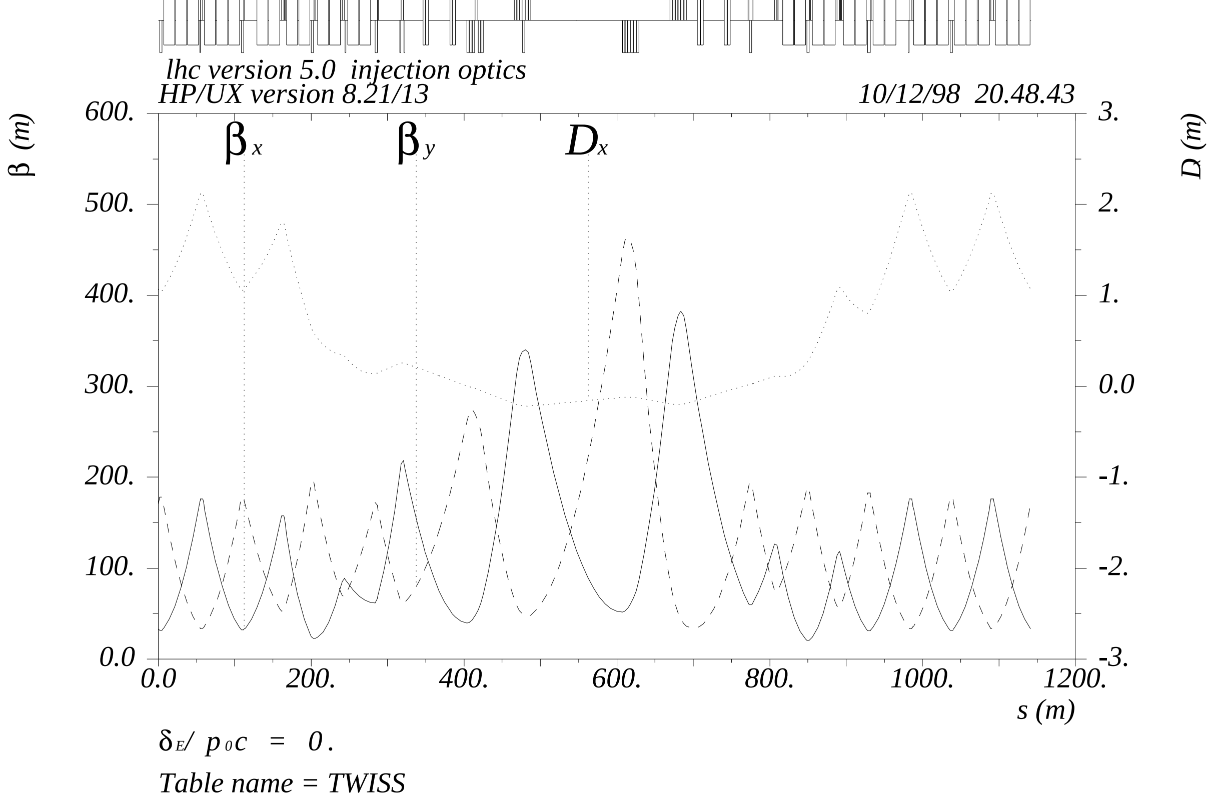

Fig 7: /ir7/q6cold with small or zero symmetric modules (KQ4S.7 and KQ5S.7)

KQT6.R7	.0010017
KQT6.L7	-.0013008
KQ5A.7	-.0012691
KQ5S.7	.0000323
KQ4A.7	.0012600
KQ4S.7	-.0000027

KQT12.L7	-.0003196	
KQT11.L7	.0022548	
KQT10.L7	.0046966	near limit
KQT9.L7	.0003270	
KQT8.L7	-.0000308	
KQT7.L7	.0025880	

KQT11.R7	-.0000297
KQT10.R7	.0002257
KQT9.R7	.0038695
KQT8.R7	.0026197
KQT7.R7	.0032651

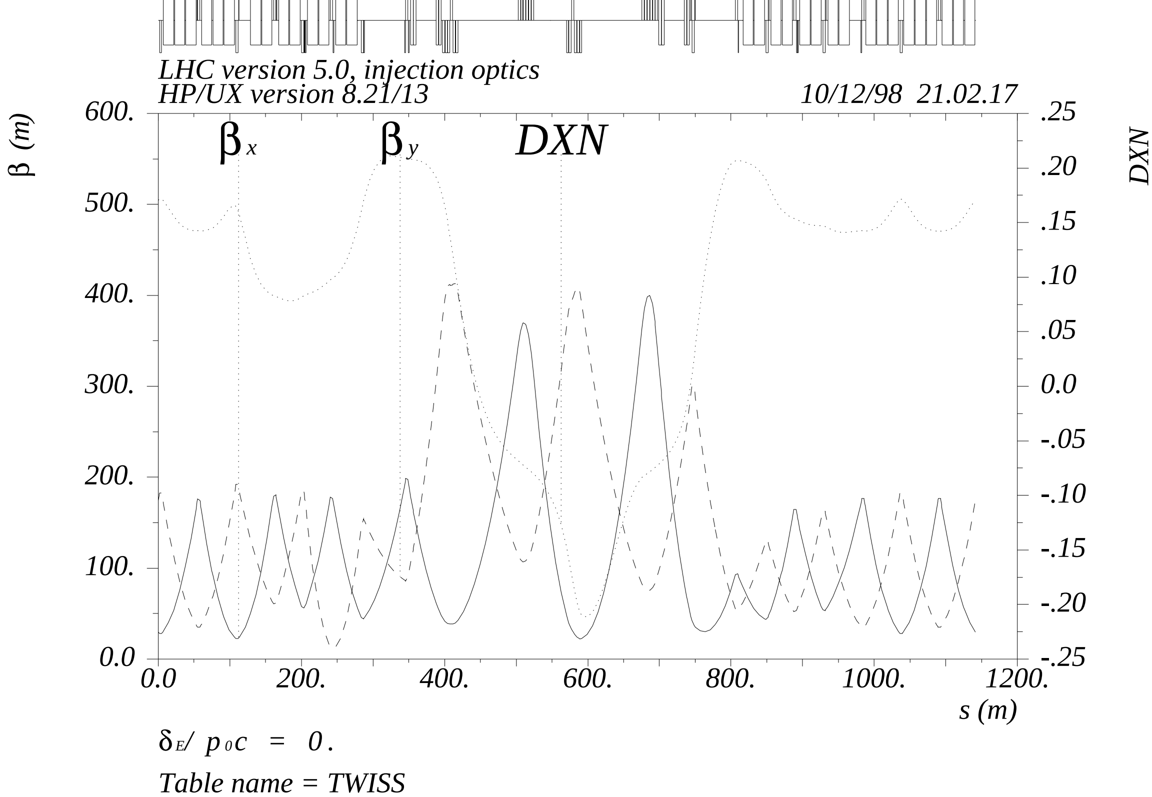

Fig 8: /ir3/q6cold; arc cell tunes mux=0.28, muy=0.24

KQT6.R3	.0026032
KQT6.L3	-.0025578
KQ5A.3	-.0013058
KQ5S.3	.0011737
KQ4A.3	.0012187
KQ4S.3	.0009719

KQT12.L3	.0042789
KQT11.L3	.0026561
KQT10.L3	.0001054
KQT9.L3	-.0038791
KQT8.L3	-.0016799
KQT7.L3	-.0020801

KQT11.R3	-.0034836
KQT10.R3	.0005650
KQT9.R3	-.0007408
KQT8.R3	.0028728
KQT7.R3	-.0008644

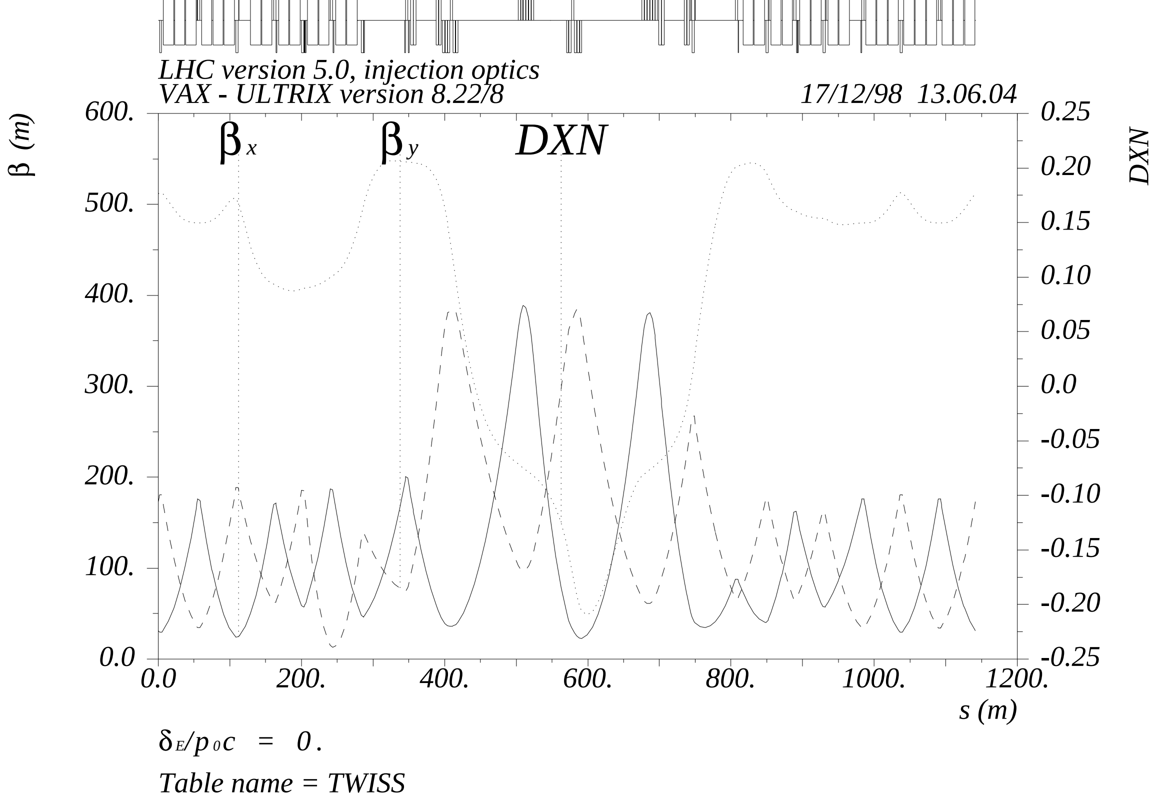

Fig 8a: /ir3/q6cold; Talman tunes: Qx=65.28, Qy=58.31

KQT6.R3	0.0029018
KQT6.L3	-0.0022577
KQ5A.3	-0.0013134
KQ5S.3	0.0010343
KQ4A.3	0.0012440
KQ4S.3	0.0008523
KQT12.L3	0.0037336
KQT11.L3	0.0028937
KQT10.L3	-0.0000870
KQT9.L3	-0.0034769
KQT8.L3	-0.0012166
KQT7.L3	-0.0025476
KQT11.R3	-0.0036473
KQT10.R3	0.0023001
KQT9.R3	-0.0005135
KQT8.R3	0.0033794
KQT7.R3	-0.0009632

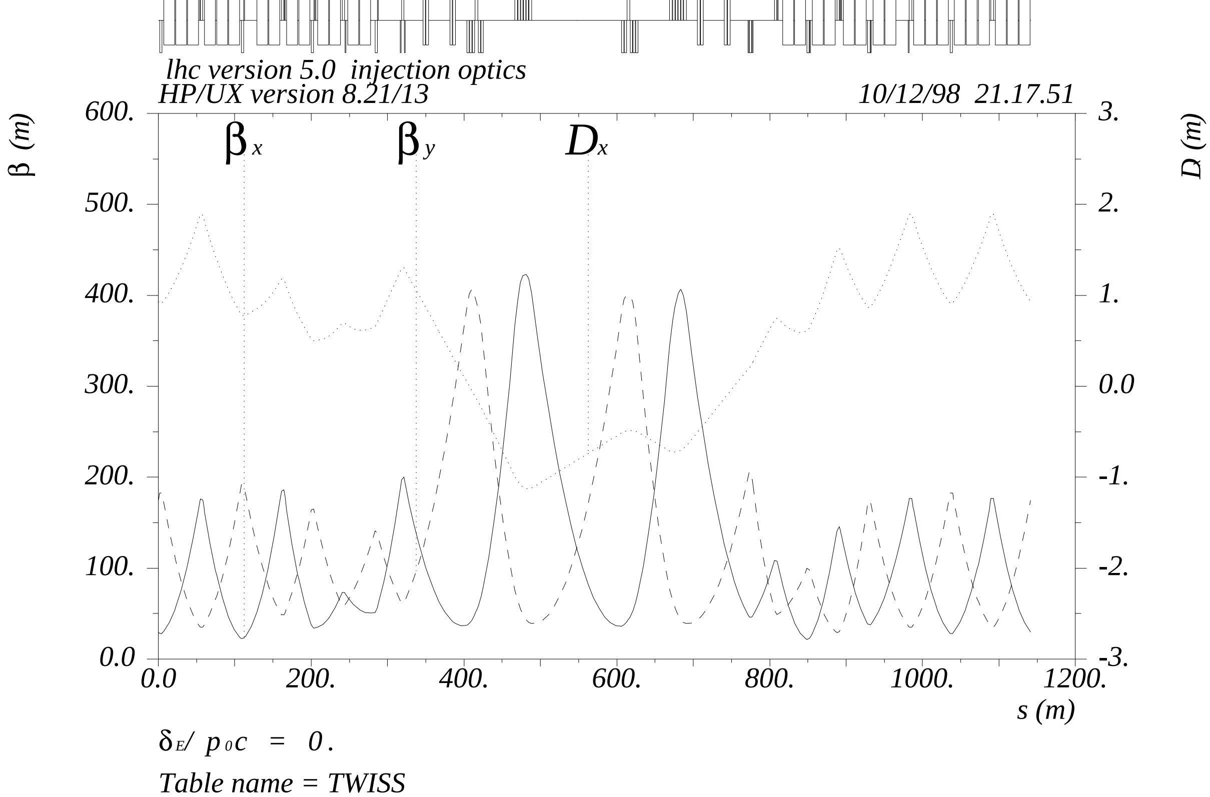

Fig 9: /ir7/q6cold; AV tunes: arc cell tunes mux=0.28, muy=0.24

KQT6.R7	-.0002568
KQT6.L7	-.0011952
KQ5A.7	-.0013527
KQ5S.7	.0001526
KQ4A.7	.0013158
KQ4S.7	.0000275
KQT12.L7	.0041601
KQT11.L7	.0014327
KQT10.L7	.0031769
KQT9.L7	.0000904
KQT8.L7	-.0039819
KQT7.L7	.0035451
KQT11.R7	-.0015264
KQT10.R7	-.0034732
KQT9.R7	.0024965
KQT8.R7	-.0011394
KQT7.R7	.0036008